Int J Heat Mass Transfer Vol 20, pp 131–139. Pergamon Press 1977 Printed in Great Britain

NATURAL CONVECTION PATTERNS IN A LONG INCLINED RECTANGULAR BOX HEATED FROM BELOW

PART II. THREE-DIMENSIONAL NUMERICAL RESULTS

HIROYUKI OZOE, KAZUMITSU YAMAMOTO* and HAYATOSHI SAYAMA
Department of Industrial and Mechanical Engineering, School of Engineering, Okayama University, Okayama, Japan

and

STUART W. CHURCHILL
Department of Chemical and Biochemical Engineering, University of Pennsylvania, Philadelphia, PA 19174, U.S.A.

(*Received* 30 *October* 1975 *and in revised form* 19 *April* 1976)

Abstract—The partial-differential equations for the conservation of mass, momentum and energy were solved numerically in three dimensions for natural convection in a long, inclined rectangular channel with an aspect ratio (width/height) of 2.0. The channel was heated from below and cooled from above and was rotated about the long dimension. The computed particle paths for angles of inclination up to 0.1222 rad were found to be a pair of three-dimensional double spirals with oblique axes. For higher angles a two-dimensional longitudinal roll-cell was obtained. The flow patterns derived for these computations at $Ra = 4000$ and $Pr = 10$ are in good agreement with the photographs in Part I for glycerol at $Ra = 12\,000$ in a $40 \times 240 \times 20$ mm box.

NOMENCLATURE

g, acceleration due to gravity in the z-direction;
H, height of channel;
k, thermal conductivity;
Nu, average Nusselt number, $= \dfrac{qH}{k(T_h - T_c)}$;
p', dynamic pressure;
Pr, Prandtl number, $= \nu/\alpha$;
q, mean heat flux density over surface;
Ra, Rayleigh number, $= g\beta(T_h - T_c)H^3/\nu\alpha$;
t, time;
T, temperature;
T_c, temperature of cold surface;
T_h, temperature of hot surface;
T_0, initial temperature, $= (T_h + T_c)/2$;
u, velocity component in x-direction;
U, dimensionless velocity component in x-direction $= uH/\alpha$;
$\mathbf{v}$, vector velocity;
v, velocity component in y-direction;
$\mathbf{V}$, dimensionless velocity vector, $= \mathbf{v}H/\alpha$;
V, dimensionless velocity component in y-direction, $= vH/\alpha$;
w, velocity component in z-direction;
W, dimensionless velocity component in z-direction, $= wH/\alpha$;
x, distance across channel;
X, dimensionless coordinate, $= x/H$;
y, distance along channel;
Y, dimensionless coordinate, $= y/H$;
z, distance downward through channel;
Z, dimensionless coordinate, $= z/H$.

Greek letters

α, thermal diffusivity;
β, volumetric coefficient of expansion with temperature;
θ, angle of inclination of x-axis from horizontal;
ν, kinematic viscosity;
ρ_0, density at T_0;
τ, dimensionless time, $= t\alpha/H^2$;
Φ, dimensionless temperature, $= (T - T_0)/(T_h - T_c)$;
$\boldsymbol{\psi}$, dimensionless vector potential [see equation (10)];
$\boldsymbol{\Omega}$, dimensionless vorticity vector [see equation (9)].

INTRODUCTION

IN PART I of this paper [1] photographs of the convective motion in glycerol in an inclined $40 \times 240 \times 20$ mm box were taken at several depths in all three orthogonal planes. The box was heated from below and cooled from above at conditions corresponding to $Ra \cong 12\,000$ and $Pr = 2720$–3000. The variation in the rate of heat transfer was shown to bear a close correspondence to the several observed modes of circulation.

Part II presents the results of a numerical solution of a three-dimensional mathematical model representing essentially the same problem studied experimentally in Part I. The model is for an infinitely long channel rather than the box of finite dimensions and the calculations are for $Ra = 4000$ and $Pr = 10$. The infinite length is not expected to change the behavior significantly from the 12/1 ratio of length-to-height for the box. The lower Rayleigh number was chosen to mini-

*K. Yamamoto is currently with Kobe Steel, Ltd., Kobe, Japan.

mize instability in the numerical calculations and the error due to the use of a finite grid-size. The rate of heat transfer is thereby decreased significantly but the transitions in the rate of heat transfer have been observed [2, 3] to be relatively insensitive to Ra. This value of Pr was chosen as an approximation for all fluids with $Pr \geqslant 0.7$, including glycerol.

MATHEMATICAL MODEL AND METHOD

The geometrical configuration of the model is shown in Fig. 1. The length of the fluid cell in the y-direction is postulated to be equal to the height H. The mathematical model is the same as that described by Ozoe *et al.* [4, 5] for a square channel, except for the modification in the boundary conditions corresponding to the greater width ($2H$) of the channel. This model incorporates the Boussinesq approximations of negligible variation in physical properties, except for the density in the buoyancy terms, and negligible viscous dissipation, and is thus

$$\nabla \cdot \mathbf{v} = 0 \tag{1}$$

$$\frac{\partial T}{\partial t} = \alpha \nabla^2 T \tag{2}$$

$$\frac{\partial u}{\partial t} = -\frac{1}{\rho_0}\frac{\partial p'}{\partial x} + \nu \nabla^2 u + g\beta \sin\theta (T - T_0) \tag{3}$$

$$\frac{\partial v}{\partial t} = -\frac{1}{\rho_0}\frac{\partial p'}{\partial y} + \nu \nabla^2 v \tag{4}$$

and

$$\frac{\partial w}{\partial t} = -\frac{1}{\rho_0}\frac{\partial p'}{\partial z} + \nu \nabla^2 w - g\beta \cos\theta (T - T_0). \tag{5}$$

Introducing the vector potential and vorticity, following Aziz and Hellums [6], these equations can be reduced to the following more tractable dimensionless equations:

$$\nabla \cdot \psi = 0 \tag{6}$$

$$\frac{\partial \Phi}{\partial \tau} = \nabla^2 \Phi \tag{7}$$

and

$$\frac{1}{Pr}\left[\frac{\partial \Omega}{\partial \tau} - (\Omega \cdot \nabla)\mathbf{V}\right] = Ra \begin{pmatrix} -\dfrac{\partial \Phi}{\partial Y}\cos\theta \\ \dfrac{\partial \Phi}{\partial Z}\sin\theta + \dfrac{\partial \phi}{\partial X}\cos\theta \\ -\dfrac{\partial \Phi}{\partial X}\sin\theta \end{pmatrix} + \nabla^2 \Omega \tag{8}$$

where

$$\Omega \equiv \nabla X \mathbf{V} = -\nabla^2 \psi \tag{9}$$

and

$$\mathbf{V} \equiv \nabla X \psi. \tag{10}$$

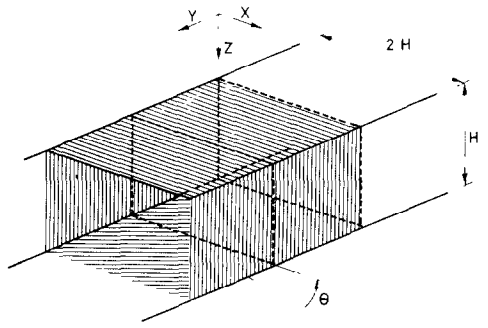

FIG. 1. Geometrical configuration of model.

The appropriate boundary conditions are

$$\frac{\partial \psi_x}{\partial X} = \psi_y = \psi_z = \Omega_x = 0, \quad \Omega_y = -\frac{\partial W}{\partial X}, \quad \Omega_z = \frac{\partial V}{\partial X} \quad \text{at} \quad X = 0 \text{ and } 2 \tag{11}$$

$$\psi_x = \frac{\partial \psi_y}{\partial Y} = \psi_z = \frac{\partial^2 \psi_x}{\partial Y^2} = \frac{\partial^2 \psi_z}{\partial Y^2} = \Omega_x = \Omega_z = 0 \quad \text{at} \quad Y = 0 \text{ and } 1 \tag{12}$$

$$\psi_x = \psi_y = \frac{\partial \psi_z}{\partial Z} = \Omega_z = 0, \quad \Omega_x = -\frac{\partial V}{\partial Z}, \quad \Omega_y = \frac{\partial U}{\partial Z} \quad \text{at} \quad Z = 0 \text{ and } 1. \tag{13}$$

The numerical method of solution is also identical. Equations (7) and (8) were solved by finite-difference methods using the three-dimensional ADI (alternating direction-implicit method) developed by Brian [7]. The first and second derivatives in space were approximated by central differences and the time-derivatives by a first-order difference. The steady state solution was obtained as the limit of a transient calculation. The three components of the vector potential were obtained from equation (9) using a fictitious unsteady term for ψ as proposed by Samuels and Churchill [8]. In this application 17 grid-points were used in the X-direction and 9 in the Y- and Z-directions, resulting in $\Delta X = \Delta Y = \Delta Z = 0.125$.

NUMERICAL RESULTS

Transient behavior

The numerical calculations were started from the quiescent state by a temperature shock in the fluid or from a different, previously computed steady state. The transient behavior of the mean Nusselt number over the central fluid plane and of the three components of the vector potential at the central point of the fluid cell is illustrated in Fig. 2. Case (a) is for a horizontal channel starting from the quiescent state. The values of ψ_y and ψ_z and negligible compared to ψ_x and are indistinguishable from zero in this plot, indicating that the mode of circulation is a quasi-two-dimensional roll-cell with its axis in the X-direction. Near $X = 0$ and 2 (not plotted) ψ_y and ψ_z have a magnitude comparable to ψ_x owing to the three-dimensional motion generated by the drag of the side walls.

Case (b) of Fig. 2 is for 0.0524 rad of inclination starting from the quiescent state. ψ_y and ψ_z are no longer negligible and the steady Nusselt number is slightly less than that for no inclination. Case (c) is for 0.0873 rad of inclination starting from the steady state for 0.0524 rad. ψ_x and Nu decrease while ψ_y and ψ_z increase. However, ψ_x remains greater than ψ_y. Case (d) is for 0.1222 rad of inclination starting from the near-steady state at 0.0873 rad. The calculations were halted at $\tau = 0.7$ (700 time iterations) to save computer time. However previous experience [5] has shown that once ψ_x falls below ψ_y in this type of problem it continues to decrease to zero, indicating transition to a two-dimensional longitudinal roll-cell. The decrease in Nu as the angle of inclination is increased up to 0.1222 rad is in general agreement with the experimental observations of Ozoe *et al.* [2] and Arnold *et al.* [3, 9].

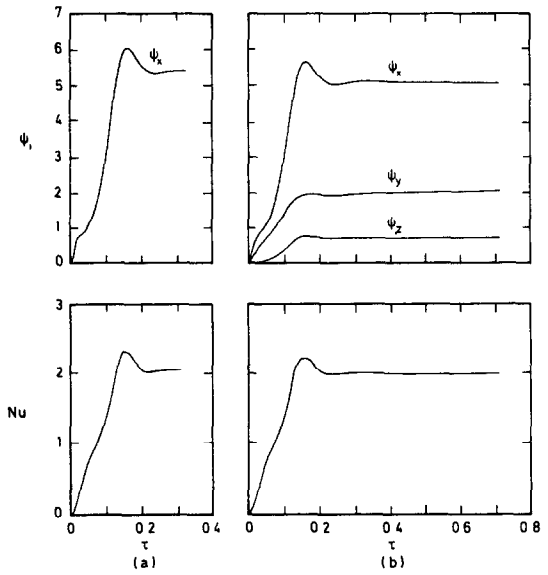

Fluid particle paths

Traces of the streak-lines for fluid particles starting at $X = 0.125$ or 0.25 and $Y = Z = 0.1875$ are shown in Figs. 3–6 for these same four cases. Figure 3 which is for the horizontal case indicates a spiral, first decreasing, then increasing and finally decreasing again in radius as the particle moves across the cell toward the central plane and then back to the starting point. A symmetrical motion occurs in the other half of the cell. The axial component of the motion is difficult to observe in experiments since it is an order of magnitude less than that of the other two components and since observations are usually confined to the Y–Z planes.

Figure 4, for 0.0524 rad of inclination reveals a pair of skewed, double spirals. The plane of symmetry dividing the pairs is also skewed. When viewed from the Z-direction this motion appears as a series of oblique roll-cells, alternating in direction. Figure 5, for 0.0873 rad of inclination, exhibits further skewing: in Fig. 6 for 0.1222 rad of inclination and $\tau = 0.7$ the skewing almost exceeds the diagonal of the fluid cell. Since this is a transient state the traces should be understood as the combined path of many particles. At longer times this complex circulation would degenerate to a two-dimensional, longitudinal cell. When this longidinal cell is attained the trace of a fluid particle becomes a single straight line in the X–Y and Y–Z planes and a single loop in the X–Z plane.

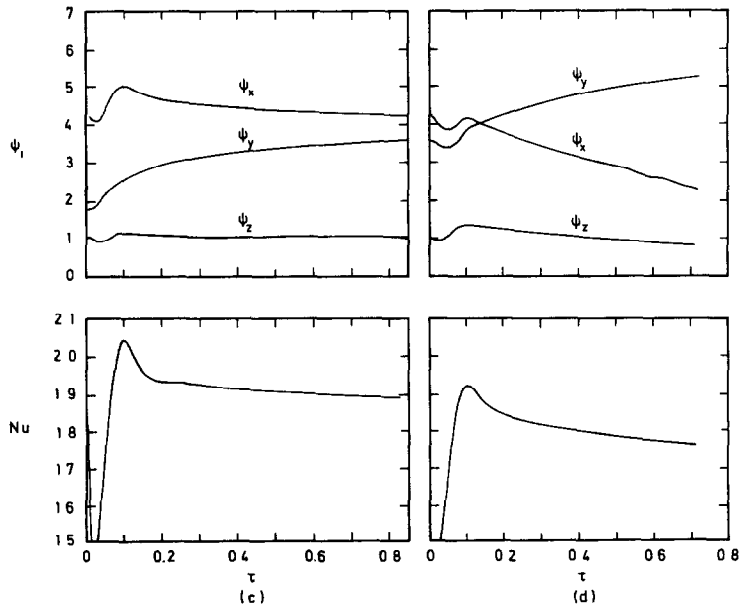

FIG. 2. Transient response of components of vector potential at central point and average Nusselt number at central plane. (a) Horizontal from quiescent state; (b) $\theta = 0.0524$ rad from quiescent state; (c) $\theta = 0.0873$ rad from $\theta = 0.0524$ rad; (d) $\theta = 0.1222$ rad from $\theta = 0.0873$ rad.

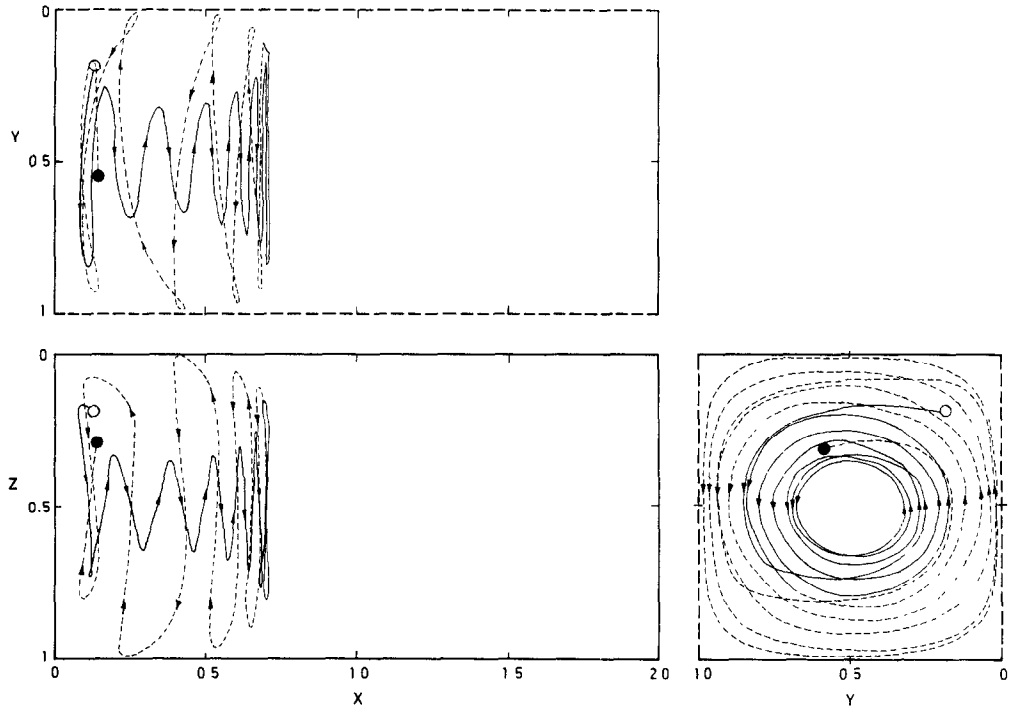

FIG. 3. Streak-line in horizontal channel. ○—starting point; ●—$\Delta\tau = 3.7$.

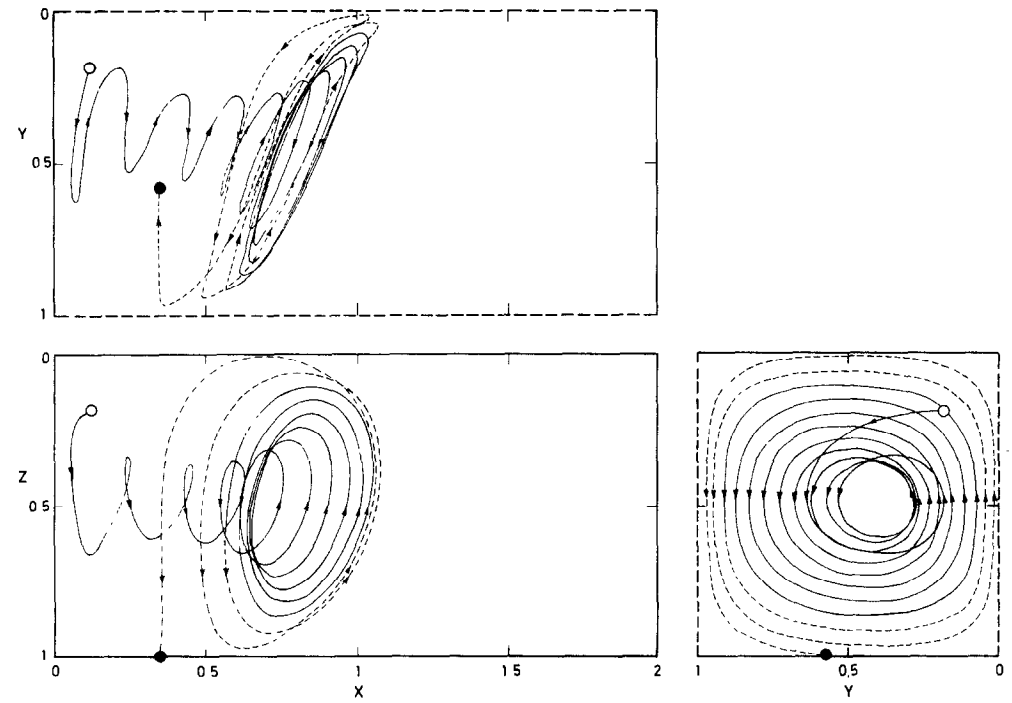

FIG. 4. Streak-line for 0.0524 rad inclination. ○—starting point; ●—$\Delta\tau = 2.875$.

Critical angle of inclination

The critical angle of inclination for transition from oblique to longitudinal cells is known experimentally (see Fig. 9 of [2]) to increase from 0 to $\pi/2$ rad with increasing aspect ratio [2, 3, 9]. The calculations and plots herein offer an explanation. As the aspect ratio increases the roll-cells can become more and mo oblique before the boundary between the half-cel exceeds the diagonal of fluid cell as suggested by t top (X–Y) view of Fig. 6. For very large aspect rati the critical angle would thereby be expected to a proach $\pi/2$ rad as observed.

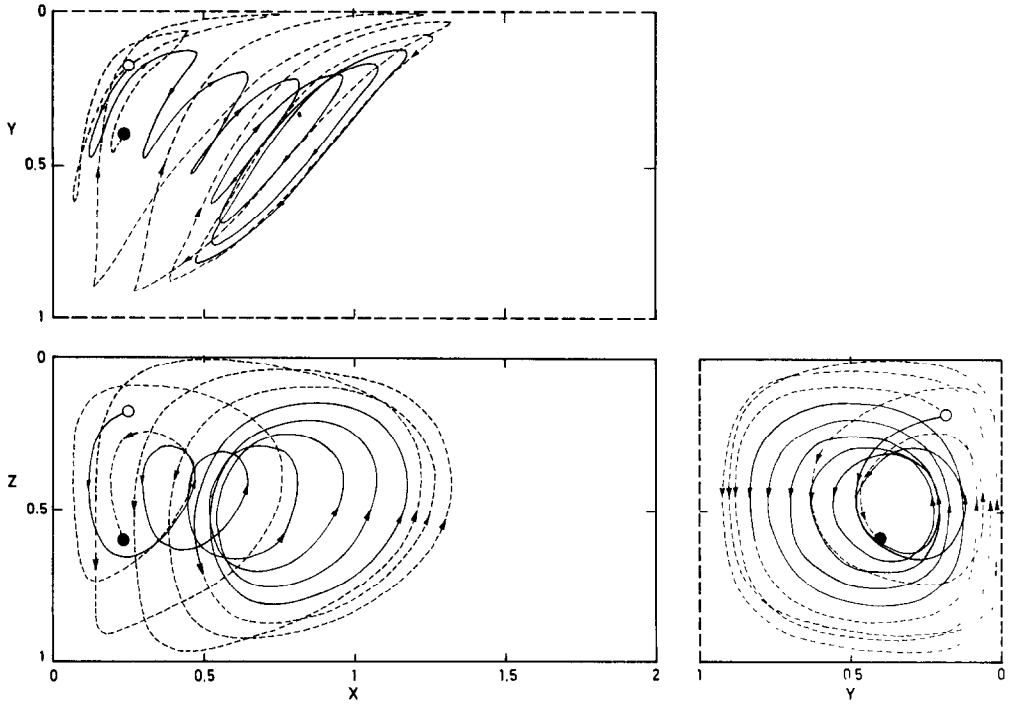

FIG. 5. Streak-line for 0.0873 rad inclination. ○—starting point; ●—$\Delta\tau = 3.4$.

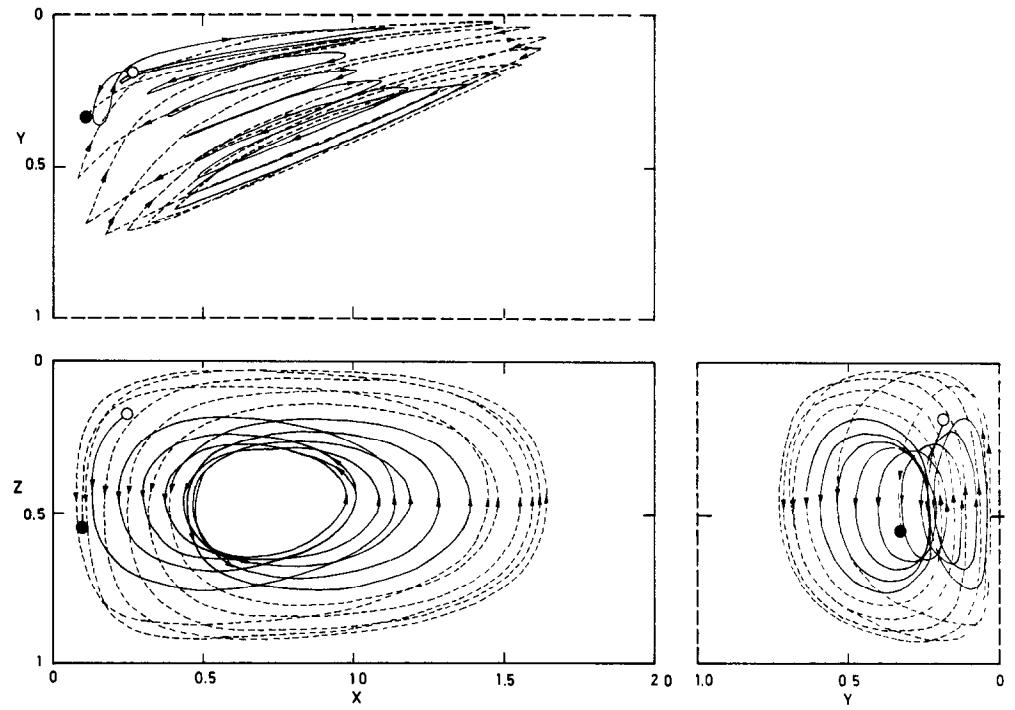

FIG. 6. Streak-line for 0.1222 rad inclination. ○—starting point; ●—$\Delta\tau = 4.275$.

Comparison with photographs

A different kind of plot must be constructed for comparison with the photographs of Part I of this paper. Figures 7–15 show short-time traces of the computed streak-lines starting from all of the grid-points in the indicated plane for comparison with the aluminum particle streaks recorded on the film. Figure 7 is for the planes of $X = 0.125, 0.50$ and 1.0 with $\theta = 0$ for a time period $\Delta\tau = 0.025$. The length of the line-segments is proportional to the combined Y–Z component of the velocity. The graph for $X = 1.0$ corresponds to Fig. 8 of Part I.

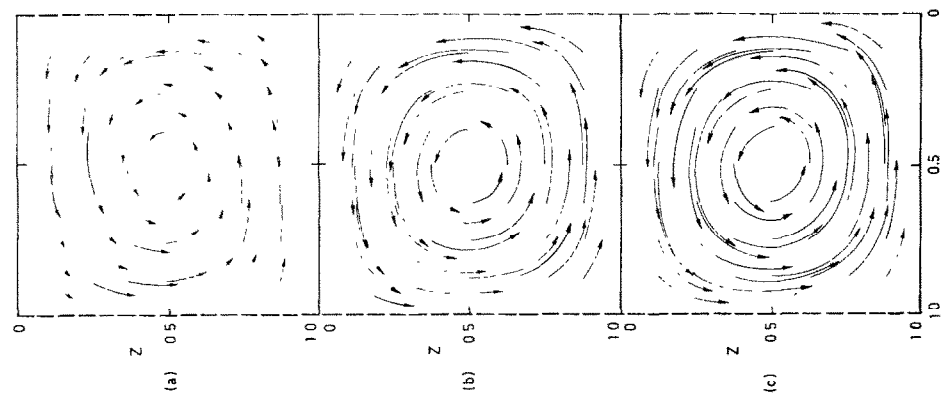

FIG. 7. Streak-lines for horizontal channel over $\Delta\tau = 0.025$. (a) $X = 0.125$; (b) $X = 0.5$; (c) $X = 1.0$.

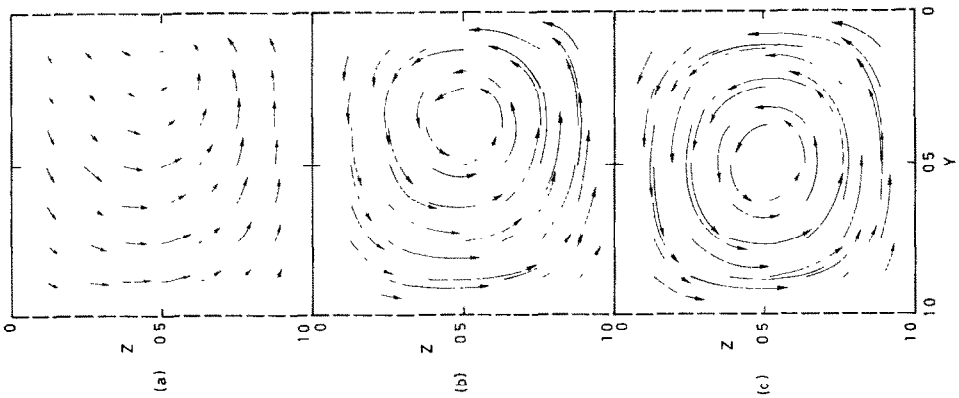

FIG. 8. Streak-lines for 0.0873 rad inclination over $\Delta\tau = 0.025$. (a) $X = 0.0625$; (b) $X = 0.5$; (c) $X = 1.0$.

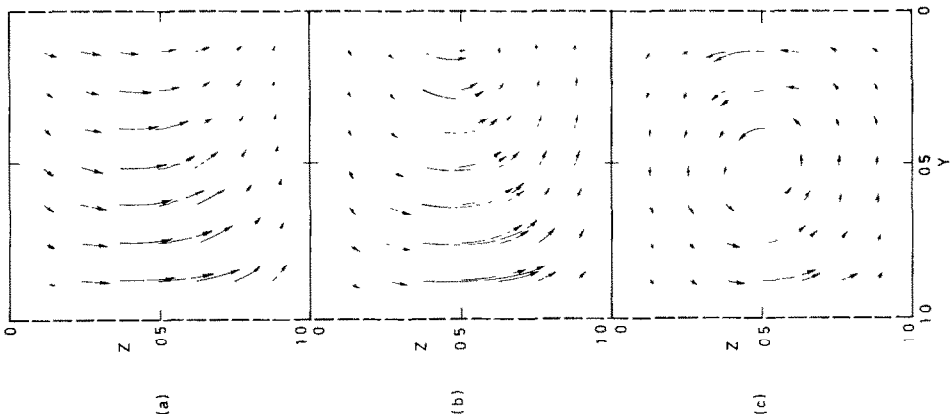

FIG. 9. Streak-lines for 0.1222 rad inclination at $\tau = 0.7$. (a) $X = 0.0625 \pm 0.0625$, (b) $X = 0.5 \pm 0.075$; (c) $X = 1.0 \pm 0.075$.

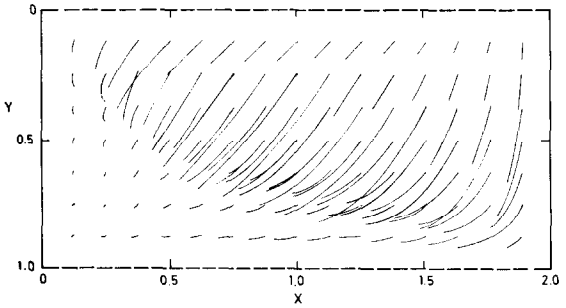

FIG. 10. Streak-lines for 0.0873 rad inclination over $\Delta\tau = 0.05$ in $Z = 0.35 \pm 0.125$.

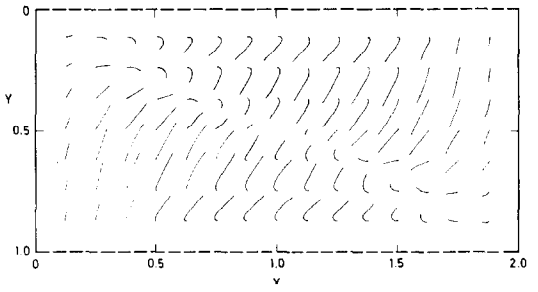

FIG. 13. Streak-lines for 0.0873 rad inclination over $\Delta\tau = 0.025$ in the $Z = 0.5$ plane.

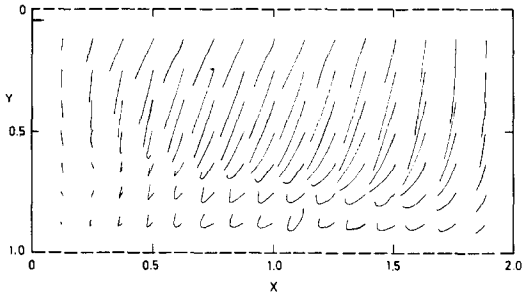

FIG. 11. Streak-lines for 0.0524 rad inclination over $\Delta\tau = 0.05$ in $Z = 0.35 \pm 0.125$.

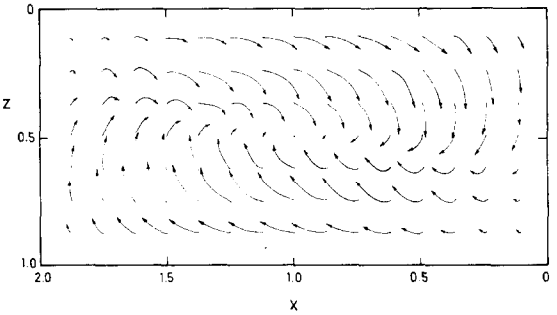

FIG. 14. Streak-lines for 0.0524 rad inclination over $\Delta\tau = 0.025$ in the $Y = 0.5$ plane.

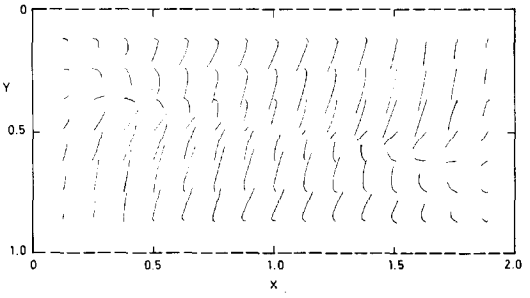

FIG. 12. Streak-lines for 0.0524 rad inclination over $\Delta\tau = 0.025$ in the $Z = 0.5$ plane.

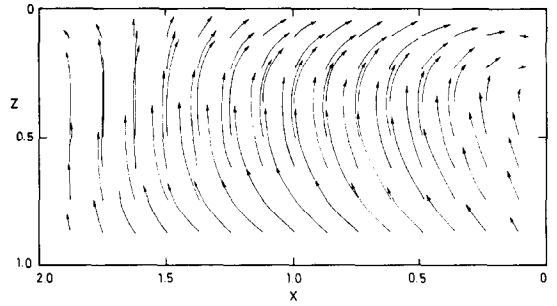

FIG. 15. Streak-lines for 0.0524 rad inclination over $\Delta\tau = 0.025$ in the $Y = 0.125$ plane.

Figure 8 is for 0.0873 rad of inclination over $\Delta\tau = 0.025$. For points starting in the plane $X = 0.0625$, the center of circulation is seen to be near the $Y = 0$ plane, i.e. the fluid interface with the adjacent fluid cell, and corresponds approximately to Fig. 14 of Part I. The plot (not shown) for $X = 1.9375$ is the same as that for $X = 0.0625$ except that it is rotated π rad and thus corresponds to the alternate cells pictured in Fig. 14 of Part I. For points starting in the plane $X = 0.5$, the center of circulation is seen to be near $Z = 0.5$, $Y = 0.375$ in agreement with Fig. 15—Part I. The plot (not shown) for $X = 1.5$ is the same as that for $X = 0.5$ except that it is rotated π rad and thus corresponds to Fig. 17—Part I. For the plane $X = 1.0$ the center of circulation is near $Y = Z = 0.5$ in agreement with Fig. 16—Part I. The slight discrepancies between the computed and experimental results may be due to heat leakage through the insulation.

Figure 9 is for the transient state at $\tau = 0.7$ for 0.1222 rad of inclination. The indicated width of X corresponds to the 3 mm width of the illumination used in Part I. The deviation of the streak-lines from the vertical indicates the still incomplete transition to a longitudinal cell which is attained at the steady state.

Figure 10 is for 0.0873 rad of inclination over $\Delta\tau = 0.05$ in the region $Z = 0.35 \pm 0.125$ and corresponds to Figs. 12 and 13 of Part I. Since the laser beam used in taking these photographs travelled in the decreasing X-direction, the brightest regions should occur where the aluminum flakes are moving vertically, normal to the beam or in the $Y = -X$ direction. Conversely the aluminum flakes flowing horizontally in the direction of the beam reflect the least light into the camera. These expectations are confirmed. The short streaks and long streaks in Fig. 10 correspond to the light and dark areas, respectively, in Figs. 12 and 13 of Part I. The computed values can thus be used to explain the "bell-shapes" of the photographs.

Figure 11 is for 0.0524 rad of inclination but otherwise for the same conditions as in Fig. 10. Figure 9

is the corresponding photograph of Part I. Figure 11 can again be used to explain the light and dark patterns.

Figures 12 and 13 are for 0.0524 and 0.0873 rad of inclination in the $Z = 0.5$ plane. Photographs were not taken for this condition but a light streak would be expected along $Y = 0.5$ in the first case and along the X–Y diagonal in the second.

Figures 14 and 15 are for the $Y = 0.50$ and 0.125 planes at 0.0524 rad of inclination over $\Delta\tau = 0.025$. The flow patterns in Figs. 14 and 15 also correspond very well to those in Figs. 10 and 11 of Part I.

CONCLUSIONS

The three-dimensional flow patterns obtained by numerical integration are in excellent agreement with those obtained photographically in Part I, despite the three-fold difference in Rayleigh number, the somewhat different Pr and the finite length of the box. This agreement is a confirmation of the validity of the mathematical model and numerical solution.

Streak-lines appear to provide the best description of the complex and changing flow pattern for various angles of inclination. Short segments of these streak-lines can be used to explain otherwise anomalous photographic results.

Acknowledgement—The authors appreciate the use of the Facom 230/60 system at the Kyoto University Computer Center.

REFERENCES

1. H. Ozoe, H. Sayama and S. W. Churchill, Natural convection patterns in a long, inclined rectangular box heated from below—Part I. Three-directional photographs, *Int. J. Heat Mass Transfer* **20**, 123–129 (1977).
2. H. Ozoe, H. Sayama and S. W. Churchill, Natural convection in an inclined rectangular channel at various aspect ratios and angles—experimental measurements, *Int. J. Heat Mass Transfer* **18**, 1425–1431 (1975).
3. J. N. Arnold, I. Catton and D. K. Edwards, Experimental investigation of natural convection in inclined rectangular regions of differing aspect ratios, ASME Paper 75-HT-62 (1975).
4. H. Ozoe, K. Yamamoto, S. W. Churchill and H. Sayama, Three-dimensional numerical analysis of laminar natural convection in a confined fluid heated from below, *J. Heat Transfer* **98C**, 202–207, 519 (1976).
5. H. Ozoe, K. Yamamoto and S. W. Churchill, Three-dimensional numerical analysis of laminar natural convection in an inclined channel with a square cross-section, in review.
6. K. Aziz and J. D. Hellums, Numerical solution of the three-dimensional equation of motion for laminar convection, *Physics Fluids* **10**, 314–324 (1967).
7. P. L. T. Brian, A finite difference method of high-order accuracy for the solution of three-dimensional transient heat conduction, *A.I.Ch.E. Jl* **7**, 367–370 (1961).
8. M. R. Samuels and S. W. Churchill, Stability of a fluid in a rectangular region heated from below, *A.I.Ch.E. Jl* **13**, 77–85 (1967).
9. J. N. Arnold, P. N. Bonaparte, I. Catton and D. K. Edwards, Experimental investigation of natural convection in a finite rectangular region inclined at various angles from 0° to 180°, in *Proceedings of the 1974 Heat Transfer and Fluid Mechanics Institute, June* 1974. Stanford University Press, Stanford, CA (1974).

CONFIGURATIONS DE CONVECTION NATURELLE DANS UNE LONGUE CAVITE RECTANGULAIRE INCLINEE ET CHAUFFEE PAR LE DESSOUS—II. RESULTATS NUMERIQUES EN TRIDIMENSIONNEL

Résumé—On a résolu numériquement et dans les trois dimensions les équations aux dérivées partielles de conservation de la masse, de la quantité de mouvement et de l'énergie dans le cas d'un écoulement de convection naturelle dans un long canal rectangulaire incliné présentant un rapport largeur/hauteur égal à 2,0. Le canal est chauffé par le dessous et refroidi par le dessus et peut tourner autour de sa longue dimension. Les trajectoires calculées des particules pour des angles d'inclinaison allant jusqu'à 0,1222 rad se présentent comme une paire de spirales doubles tridimensionnelles à axes obliques. Pour des angles supérieurs un tourbillon cellulaire bidimensionnel longitudinal est obtenu. Les configurations d'écoulement obtenues par calcul numérique à $Ra = 4000$ et $Pr = 10$ sont en bon accord avec les photographies données dans la première partie pour du glycerol à $Ra = 12000$ dans une cavité de dimension $40 \times 240 \times 20$ mm.

NATÜRLICHE KONVEKTIONS-STRUKTUREN IN EINEM LANGEN, GENEIGTEN, RECHTECKIGEN BEHÄLTER, DER VON UNTEN BEHEIZT WIRD—II DREIDIMENSIONALE, NUMERISCHE ERGEBNISSE

Zusammenfassung—Für die natürliche Konvektion in einem langen, geneigten, rechteckigen Kanal mit einem Seitenverhältnis Breite: Höhe von 2:1 wurden die partiellen Differentialgleichungen für die Stoff-, Impuls- und Energiebilanz für alle drei Koordinatenrichtungen numerisch gelöst. Der Kanal wurde von unten beheizt und von oben gekühlt und rotierte um die Längsachse. Für Neigungswinkel bis zu 0,1222 rad ergab die Berechnung ein Paar dreidimensionaler, doppelter Spiralen mit schrägen Achsen. Für größere Neigungswinkel ergab sich eine zweidimensionale Längs-Rollzelle. Die für $Ra = 4000$ und $Pr = 10$ berechneten Strömungsstrukturen stimmen gut mit den in Teil I fotografierten Strukturen für Glyzerin bei $Ra = 12000$ in einem Behälter mit den Abmessungen $40 \times 240 \times 20$ mm überein.

СТРУКТУРЫ СВОБОДНОЙ КОНВЕКЦИИ В ДЛИННОЙ НАКЛОННОЙ ПРЯМОУГОЛЬНОЙ КЮВЕТЕ, НАГРЕВАЕМОЙ СНИЗУ — II. ЧИСЛЕННЫЕ РЕЗУЛЬТАТЫ ДЛЯ ТРЕХМЕРНОГО СЛУЧАЯ

Аннотация — Приведены результаты численного решения трехмерных дифференциальных уравнений в частных производных-сохранения массы, количества движения и энергии — при естественной конвекции в длинной наклонной прямоугольной кювете с отношением ширины к высоте, равным 2,0. Кювета нагревалась снизу и охлаждалась сверху и поворачивалась относительно своей продольной оси. Найдено, что при углах наклона до 0,1222 рад. расчетные траектории частиц представляли собой пару трехмерных двойных спиралей с наклонными осями. Для больших значений угла получен вихрь в виде двухмерной продольной ячейки. Структуры течения, полученные в этих расчетах при $Ra = 4000$ и $Pr = 10$, хорошо согласуются с фотографиями, представленными в 1 части для глицероля в кювете размерами $40 \times 240 \times 20$ мм при $Ra = 12\,000$.